Electronic Supplementary Information (ESI)

Control over the spatial correlation of silica perforations in thin films as a function of solution conditions

Julien Castets,[a] Louise Labeyrie,[a] Estelle Morvan,[b] David Montero,[c] Lucien Roach,[a,†] and Glenna L. Drisko[a,†]

[a] CNRS, Univ. Bordeaux, Bordeaux INP, ICMCB, UMR 5026, F-33600 Pessac, France.
[b] Institut Européen de Chimie et Biologie, UAR3033 CNRS, Université de Bordeaux, INSERM US01, Pessac 33600, France
[c] Sorbonne Université, Fédération de Chimie et Matériaux de Paris-Centre, FR 2482, 75252 Paris, France
† Corresponding author: lucien.roach@ens-lyon.fr; glenna.drisko@icmcb.cnrs.fr.

EXPERIMENTAL SECTION

Reagents and materials.

Cetyltrimethylammonium chloride (CTAC, ≥ 98.0 %, Sigma-Aldrich), cetyltrimethylammonium bromide (CTAB, ≥ 98 %, Sigma-Aldrich), hydrochloric acid (HCl, 37 wt. % in H_2O, Scharlau), nitric acid (HNO_3, 65 wt. % in H_2O, Scharlau), hydrobromic acid (HBr, 48 wt. % in H_2O, Thermo Scientific), ethanol (≥ 99.8 %, Sigma-Aldrich), tetraethyl orthosilicate (TEOS, 98 %, Thermo Scientific), strontium dichloride hexahydrate ($SrCl_2.6H_2O$, 99+ %, Thermo Scientific) and strontium dibromide ($SrBr_2$, 99.995 %, Sigma-Aldrich) were used in the fabrication of the perforated silica films. The chemicals were used as purchased without any further purification. Water was purified using a type 1 Milli-Q water system (18.2 MΩ cm).

Boron-doped prime CZ Si wafers with <100> orientation were purchased from Si-mat and used as substrates.

Fabrication of perforated SiO$_2$ films.

The protocol followed to prepare the sol-gel solutions was adapted from a previously published work[1]. In a standard synthesis (of a 0 mol% Br⁻ solution), CTAC (0.736 g, 2.3 mmol) was dissolved in ethanol (18.9 g, 410 mmol), 37 wt.% HCl (1.6 g, 16.24 mmol H⁺, 55.95 mmol H_2O). TEOS (3.4 g, 16.32 mmol) was added dropwise and the solution was aged overnight. A 2 M $SrCl_2$ solution (250 μL, 0.5 mmol Sr^{2+}) was added just before the film deposition, with the necessary amount of water

Table S1 Preparation of the solution for a bromide ion molar fraction of 0, 10, 20, 25, 50, 100 mol% Br⁻. The reagents H_2O, 2 M $SrCl_2$ and 2 M $SrBr_2$ solutions were added just before dip-coating to deposit the perforated silica film.

	mol% Br⁻	0	10	20	25	50	100
TEOS	mass (g)	3.4	3.4	3.4	3.4	3.4	3.4
	mole (mmol)	16.32	16.32	16.32	16.32	16.32	16.32
CTAC	mass (g)	0.74	0.74	0.74	0.74	0.74	-
	mole (mmol)	2.3	2.3	2.3	2.3	2.3	-
CTAB	mass (g)	-	-	-	-	-	0.84
	mole (mmol)	-	-	-	-	-	2.3
EtOH	mass (g)	18.9	18.9	18.9	18.9	18.9	18.9
	mole (mmol)	410	410	410	410	410	410
HCl (37 wt.%)	mass (g)	1.6	1.41	1.23	1.13	0.66	-
	mole (mmol)	16.24	14.31	12.48	11.47	6.70	-
HBr (48 wt.%)	mass (g)	-	0.33	0.64	0.80	1.6	2.74
	mole (mmol)	-	1.96	3.80	4.75	9.49	16.26
H_2O	volume (µL)	250	200	150	130	6	-
	mole (mmol)	13.88	11.10	8.33	7.22	0.33	-
$SrCl_2$ (2 M)	volume (µL)	250	250	250	250	250	-
	mole (mmol)	0.5	0.5	0.5	0.5	0.5	-
$SrBr_2$ (2 M)	volume (µL)	-	-	-	-	-	250
	mole (mmol)	-	-	-	-	-	0.5

(Table S1) to keep the water molar ratio constant across varying bromide ion molar ratios. The final molar ratio was 1 Si: 0.14 CTAX: 5.14 H_2O: 25 EtOH: 1 HX: 0.03 SrX_2, where X = Br⁻ or Cl⁻. All the solutions are very acidic, with a pH close to 0, all indistinguishable by pH-indicator strips.

In varying mol% Br⁻, a mix of 37 wt.% HCl and 48 wt.% HBr was used in order to reach the desired bromide ion molar ratio, as described in Table S1. For 100 mol% Br⁻, CTAB was used instead of CTAC, and a 2 M $SrBr_2$ solution was substituted for a 2 M $SrCl_2$ solution, in same molar quantities. The preparation of each solution, with the associated molar ratio are provided in Table S1 and S2.

Salt solutions of 2 M were prepared by weighing the appropriate amount of salt (5.33 g $SrCl_2$ or 4.96 g $SrBr_2$) into a 10 mL volumetric flask, then dissolved in purified water up to the 10 mL mark at ambient temperature. For the two salts, the aqueous solution of known salt concentration was immediately prepared after opening the freshly received chemical containers. As a precaution, the

Table S2 Molar ratio of the solution for a bromide ion molar fraction of 0, 10, 20, 25, 50, 100 mol% Br⁻, just before dip-coating deposition.

mol% Br⁻	0	10	20	25	50	100
TEOS	1	1	1	1	1	1
CTAC	0.14	0.14	0.14	0.14	0.14	-
CTAB	-	-	-	-	-	0.14
EtOH	25.14	25.14	25.14	25.14	25.14	25.14
HCl (37 wt.%)	1	0.88	0.76	0.70	0.41	-
HBr (48 wt.%)	-	0.12	0.23	0.29	0.58	1
H_2O	5.14	5.14	5.14	5.14	5.14	5.14
$SrCl_2$	0.03	0.03	0.03	0.03	0.03	-
$SrBr_2$	-	-	-	-	-	0.03

salts should be treated in a vacuum oven and stored in a desiccator prior use to avoid water absorption and respect the stoichiometry.

Silicon substrates were cleaned using the following procedure: in an ultrasonic bath, 30 min in acetone, 10 min in water, 30 min in ethanol, 10 min in water. Then, silicon substrates were exposed to a 65 wt.% HNO_3 solution for 30 min in order to oxidize the surface and rinsed and stored in water.

Substrates were cleaned with a KimTech lint-free wipe and residual fibers and dust were removed from the surface with dust-free compressed air.

Perforated silica films were deposited by dip-coating using a SolGelWay ACEdip 2.0 dip-coater. The withdrawal speed and chamber temperature were computer-controlled using ACEdip 2.0 software. The relative humidity in the chamber was controlled with a combination of dry and humidified air flow. For deposition, silicon substrates were submerged in the sol-gel solution at 10 mm s⁻¹, with a dwell time of 10 s, and withdrawn at 1 mm s⁻¹ at T = 25 °C and 40 % RH, followed by aging in the dip-coating chamber for 5 min. The films were calcined in a muffle furnace at 500 °C for 10 min to remove any organic matter, and to more fully condense the silica network. After thermal treatment, the films were immediately placed on a metallic plate for cooling.

Characterization techniques.

Scanning electron microscopy (SEM) images were obtained using either a Hitachi SU-70 or a JEOL JSM-6700F SEM. Samples were metalized with a platinum layer of 2 nm thickness to collect the top-view images. Images were acquired with 15 kV accelerating voltage. Cross-sectional images were collected without metallization. For the images on curved glass surfaces, a platinum layer of 10 nm thickness was used in order to maximize the conductivity. Images were acquired with 5 kV accelerating voltage. The quantification of the diameters, surface density and surface coverage were done on segmented top-view SEM images using the software ImageJ. The silica film thicknesses were measured on cross-sectional view SEM images. The thickness is measured from the top of the perforations to the silicon substrate on cross-sectional SEM images.

The size corrections for vertical measurements were done using the angle of observation θ and the trigonometric equation: $\cos\theta = D_m / D_c$, with D_m the measured size and D_c the corrected size. The positions 1 and 2 in Fig. S8b, indicated using arrows and crosses, are positioned at 7 mm and 11 mm from the center of the surface (dotted black line), respectively. These lead to two different observation angles θ with the tangent at the surface of 33° and 58° respectively. Fig. S8c-d are SEM images at position 1 and 2, respectively. The aspect ratios of the perforations are slightly different for the two images due to the difference in observation angle. After corrections, the aspect ratio in the two images is on average 1.04.

To quantify the degree of structural correlation, the segmented images were treated using ImageJ's 'Analyze Particles' function to identify the coordinates of each perforation center. The coordinates were then treated using a Python script, which calculated the Delaunay bond lengths, and the pair correlation function for each image. Errors bars on silica thicknesses, diameters, surface densities, surface coverages and Delaunay lengths were calculated using the standard deviation.

Solution Nuclear Magnetic Resonance (NMR) experiments were conducted on a Bruker Avance III HD nanobay spectrometer operating at 400MHz (1H) and 79,5MHz (^{29}Si) with a 5 mm diameter smartprobe. The lock was optimized using a deuterated solvent (DMSO-d6) in an internal coaxial tube. All NMR experiments were recorded at 293 K. Acquisition parameters for ^{29}Si INEPT NMR were used:

90°pulse of 8 µs, 64 scans, recycling delay of 5 s, SW = 32kHz, delays were optimized for 3JSiH = 4Hz. All NMR spectra were processed using the Bruker TopSpin software. A Lorentzian noise filtering of 3Hz was applied for Fourier transformation for NMR spectra. Chemical shifts were calibrated relative to Tetraethyloxilane (TEOS) signals (-82 ppm for ^{29}Si).
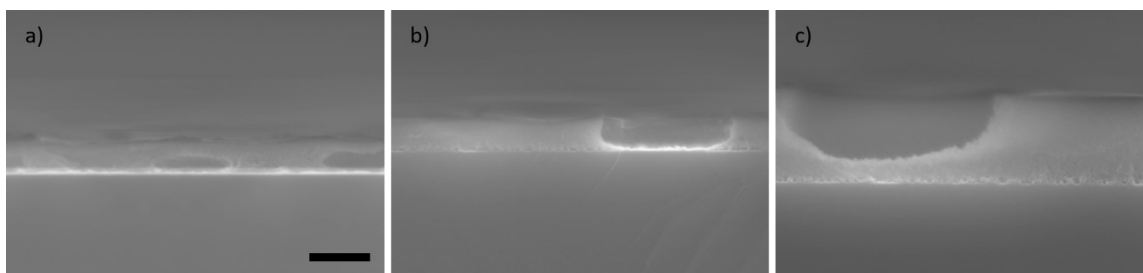
Fig. S1 Original cross-sectional images without contrast modification of perforated SiO$_2$ films on silicon substrates. Films deposited by dip-coating at 1 mm s^{-1} under 25 °C and 40 % RH with a solution composition containing a) 0, b) 10 and c) 100 mol% Br$^-$. The scale bar represents 200 nm, and the scale is equivalent for all images.
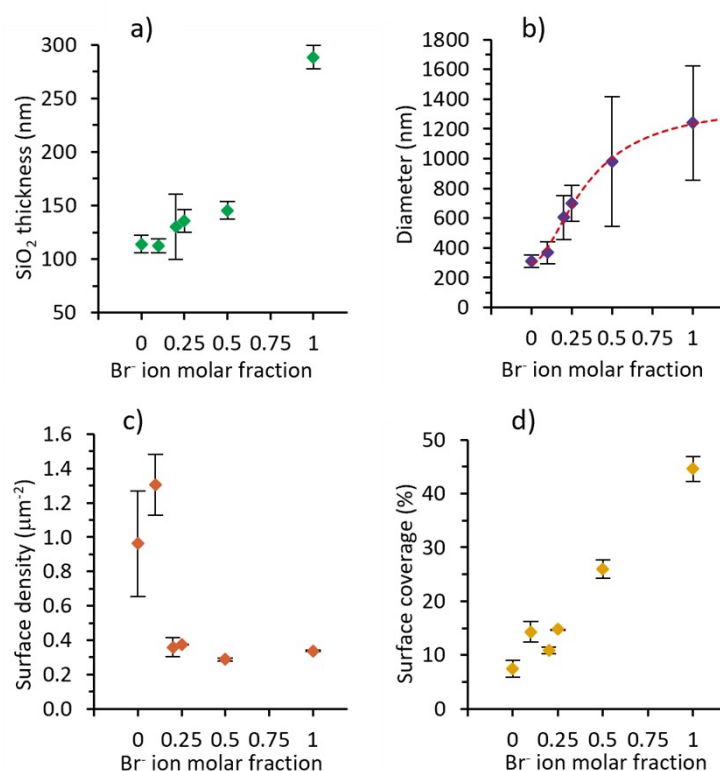
Fig. S2 Perforated SiO$_2$ thin film characteristics quantified: a) silica thickness and perforation b) diameter, c) surface density and d) surface coverage as function of the bromide ion molar fraction in the solution deposited at 1 mm s^{-1} under 25 °C and 40 % RH.

Fig. S2 displays the quantifications over the average perforation diameter, density, and surface coverage as function of the bromide ion molar fraction in the solution used for the perforated silica thin film deposition. The silica layer thickness is measured from the top of the perforations to the silicon substrate on cross-sectional SEM images (Fig. 1). The perforation diameters of each sample have been analyzed, and the distributions are presented in histograms in the Electronic Supplementary Information (Fig. S4). In most samples, a unimodal population with a certain degree of polydispersity is observed. For two samples, that of 20 and 50 mol% Br$^-$, a bimodal size population is found. However,

for both of these samples, the larger population is four times more prevalent than the smaller one. The perforation diameter only increases, non-linearly, with increasing Br$^-$ concentration, following an approximately sigmodal relationship (Fig. S2b). The perforation size increases quickly for low Br$^-$ concentrations, and then more slowly for the samples between 50 and 100 mol% Br$^-$ content. The dashed red line is a theoretical growth prediction using a logistic growth model (Fig. S2b)[2]. Logistic growth equations are used to describe the evolution in population size between a minimum and maximum size, Y_0 and Y_m respectively. In this model, the sigmoidal curve (S-shaped curve) follows the formula: $y = (Y_0-Y_m)/(1+(x/x_0)^k)+Y_m$. Where Y_0 and Y_m are respectively the initial and final sizes, x_0 is the inflection point of the curve and k is a power constant describing the growth rate defined by the derivative at $x = x_0$. Y_m represents a critical maximum value of size when the bromide ion molar fraction tends to infinity while Y_0 the average perforation size for a film fabricated with 0 mol% Br$^-$. The average diameter is well fitted by a logistic growth model (R^2 = 0.989), describing that the growth of droplets is limited by a parameter. The assumption is that the kinetic of silica gelation is the limiting parameter, as when the silica layer is fully gelled, the droplets can no longer grow.

The surface density of the perforations, define as a number of objects per surface area (μm^{-2}), is calculated on top-view SEM images by dividing the number of perforations on the image by the size of the image. Over 20 mol% Br$^-$, the surface density stabilizes around 0.3 μm^{-2} due to the change of perforation diameter. Despite a decrease in the density of the perforations, the large increase in the average perforation diameter with increasing Br$^-$ concentration leads to a net increase in the surface fraction covered by perforations (Fig. S2d). The surface fraction covered by perforations increases approximately linearly with Br$^-$ concentration, with 7 %, 26 %, and 45 % of the surface covered, respectively for the films fabricated with 0, 50, and 100 mol% Br$^-$ ion.

Silica layer thickness increases in tandem with the perforation diameter (Fig. S2a,b). We assume that the increase in silica thickness is due to an increase in the volume occupied by the perforations within the silica layer. According to this hypothesis, a constant volume of silica was deposited on the substrate during the perforated silica thin film synthesis, for all solution compositions. Simultaneously, the volume of the water droplets adsorbed within the silica increases as function of solution

conditions, leading to an increase of the overall volume of the silica layer. Then, the increase of silica thickness should be linked to the increase in volume and surface density of the perforations in each sample. The correlation between the two is provided in Electronic Supplementary Information (Fig. S3), fitted with a linear regression. The evolution of the silica layer thickness is plotted as function of ρV_p, the increase in silica layer thickness due to the volume occupied by all perforations, with ρ the surface density and V_p the volume of a single perforation, represented by half a spheroid (Fig. S3a-c).
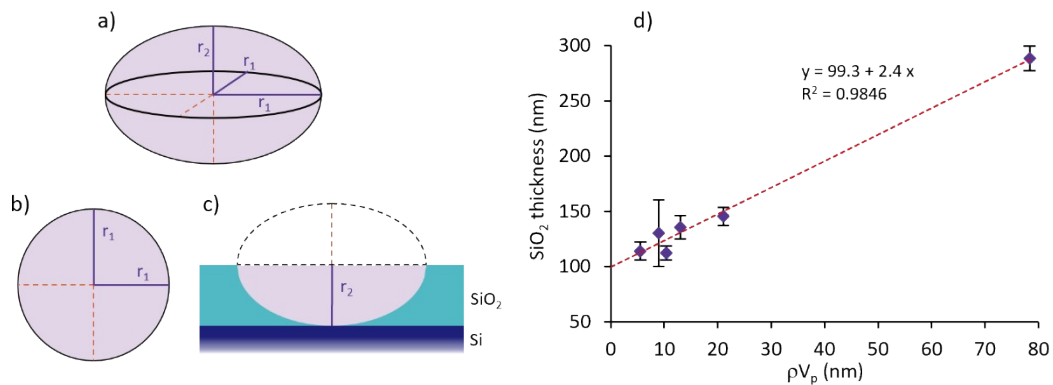
Fig. S3 Correlation between the evolution of the silica layer thickness and the increase in volume of the perforations, for films fabricated with 0, 10, 20, 25 and 50 and 100 mol% Br⁻ content. a-c) Schemes of the volume of one perforation from a) oblique, b) top-view and c) cross-sectional view. The shape of the perforation volume is comparable to half of the volume of a spheroid $V_p = \frac{4}{6}\pi r_1^2 r_2$. r_1 is the radius of a perforation, r_2 represent the perforation depth. d) Evolution of silica thickness as a function of the average volume of a perforation V_p multiplied by the associated surface density ρ. The red dashed line is a linear regression following the theoretical expression $h = h_0 + \rho V_p$, with h the thickness of a perforated silica layer, h_0 the thickness of a silica thickness deposited containing no perforations, ρ the surface density (Fig. S2c) and the volume of a single perforation V_p. The numerical equation and the fit agreement are provided.
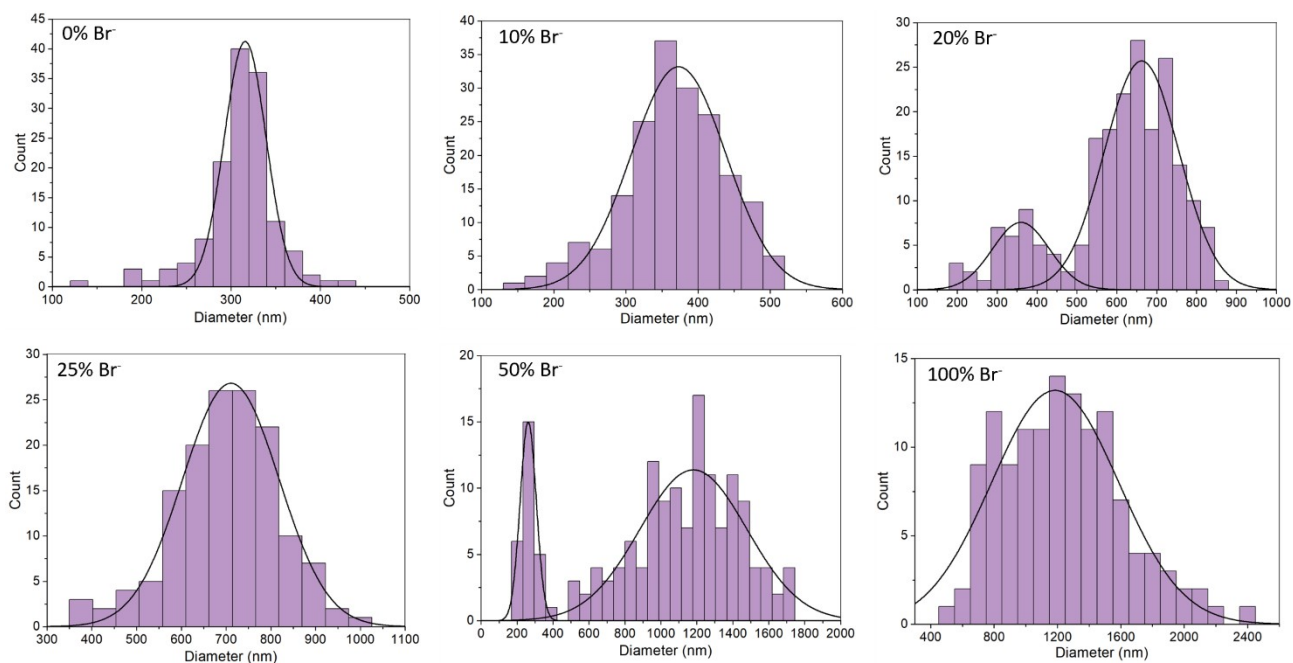
Fig. S4 Histograms of the diameter distributions of SiO_2 perforations in thin films fabricated with 0, 10, 20, 25, 50 and 100 mol% Br⁻. Solid black lines are Gaussian fits applied to the measured diameters from SEM images.
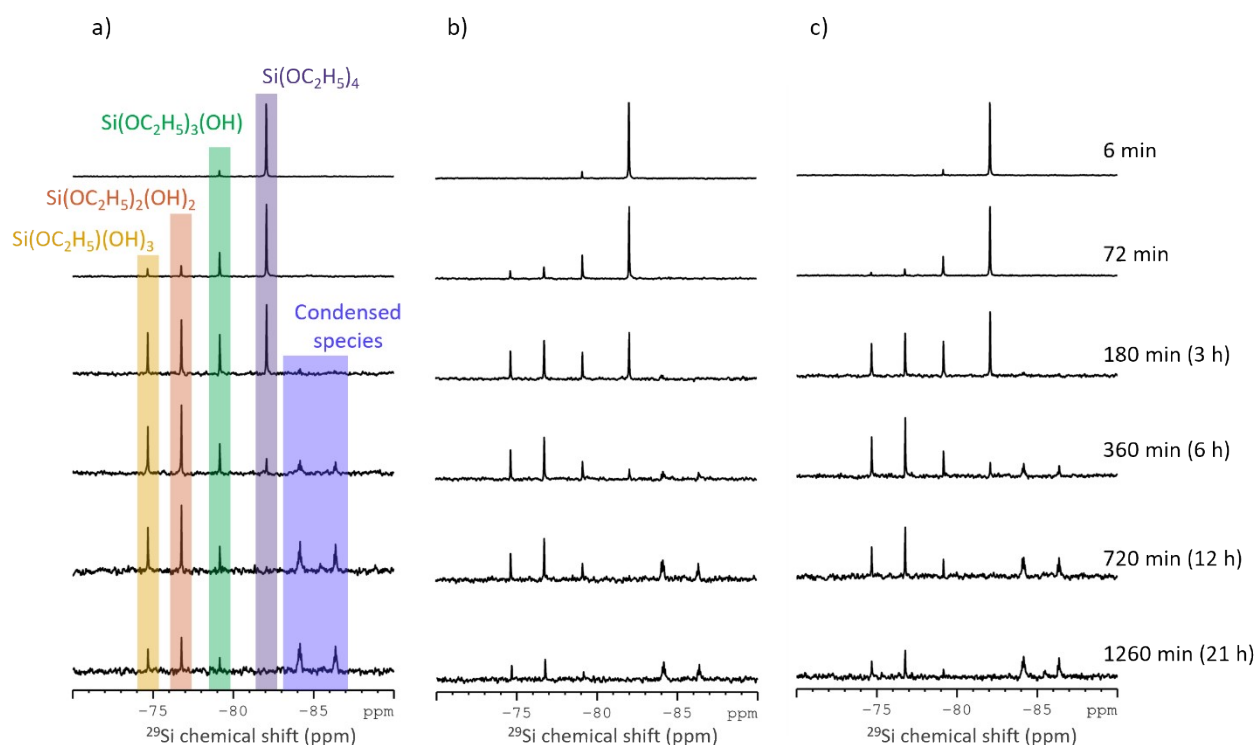

Fig. S5 Time dependence of the ^{29}Si NMR spectra for the hydrolysis of 0.56 M $Si(OC_2H_5)_4$ at 293 K, in solution containing a bromide ion molar fraction of a) 0, b) 50, c) 100 mol% Br⁻. TEOS:EtOH:H_2O molar ratios were 1:25:5, with [H⁺] = 2 × 10⁻⁴ M. Species associations to the respective chemical shifts (ppm) in a) can equally be applied to b) and c).
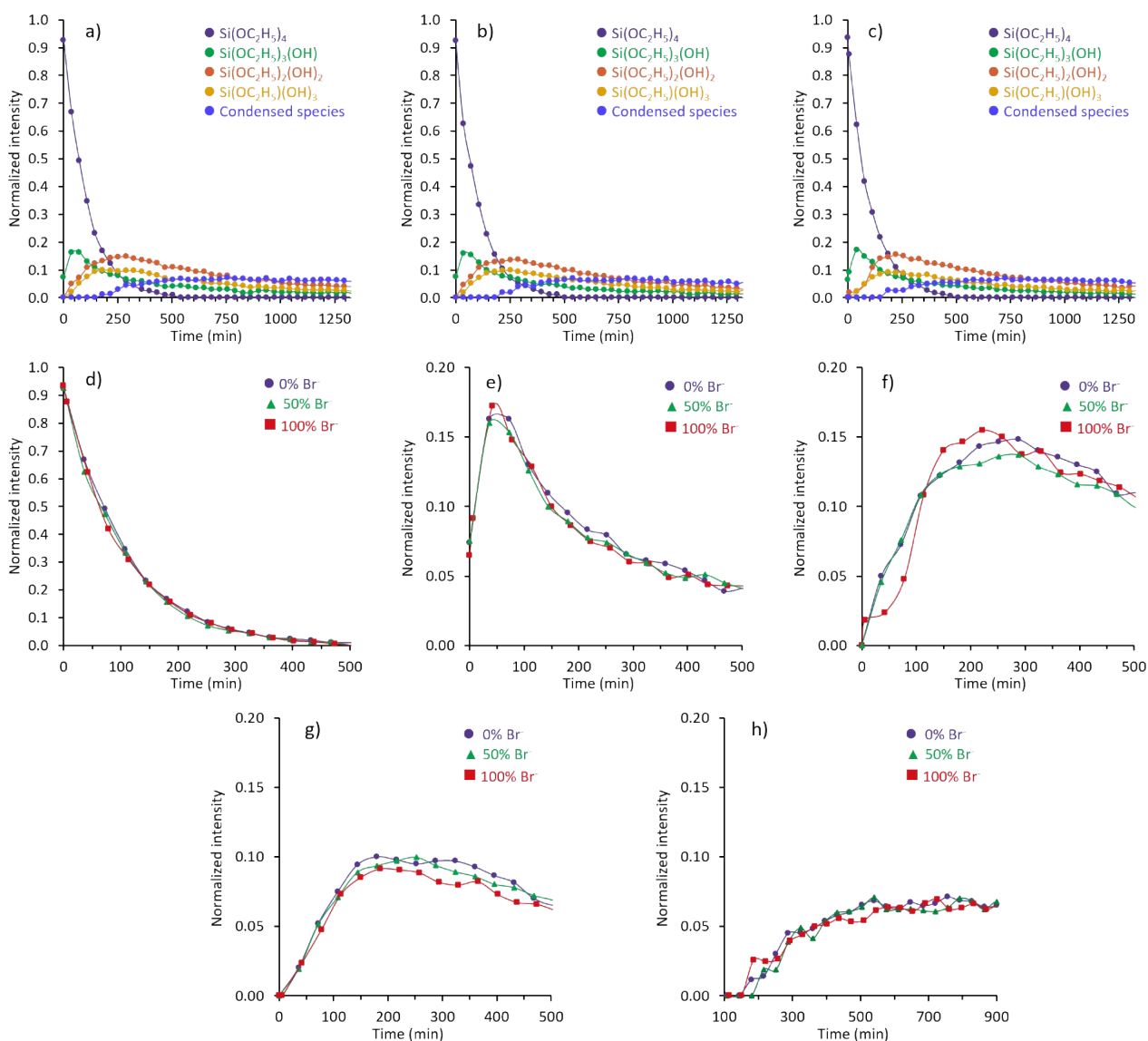
Fig. S6 Relative intensities of precursor, hydrolyzed and total condensed species as a function of reaction time with solutions containing a bromide ion molar fraction of a) 0, b) 50, c) 100 mol%. d-f) Comparison of relative intensities as a function of reaction time with solutions containing a bromide ion molar fraction (% Br⁻) of 0%, purple ●; 50%, green ▲; 100%, red ■; for d) $Si(OC_2H_5)_4$, e) $Si(OC_2H_5)_3(OH)$, f) $Si(OC_2H_5)_2(OH)_2$, g) $Si(OC_2H_5)(OH)_3$, h) condensed species. TEOS:EtOH:H_2O molar ratios were 1:25:5, with [H⁺] = 2 × 10^{-4} M. The intensities are normalized by the sum of intensities of the first spectra recorded for each solution (corresponding t = 6 min in Fig. S4).
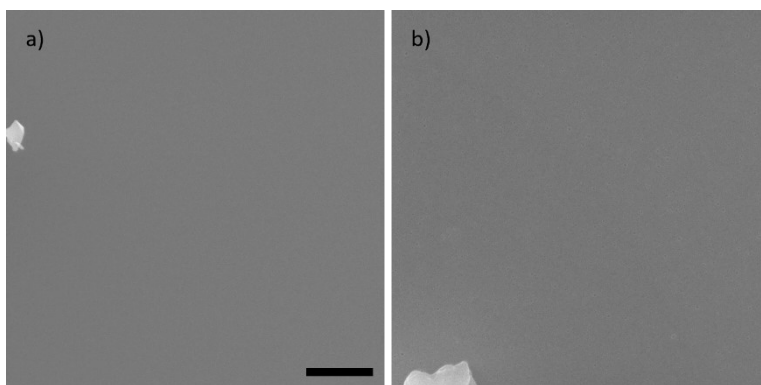
Fig. S7 SEM micrographs from the top-view of a silica layer, fabricated by dip-coating at 3 mm s^{-1} under 25 °C, a) without salt at 40 % RH, b) with a magnesium chloride salt at ~ 6 % RH. Scale bar representing 2 µm, with the scale equivalent for both images. The white objects are silicon shards due to cutting the sample for SEM observation, chosen to show the focal plane of the surface. All other parameters used for the fabrication of the two silica films in solution composition, dip-coating and thermal treatment were the same as presented in *"Fabrication of perforated SiO$_2$ films"* Electronic Supplementary Information.
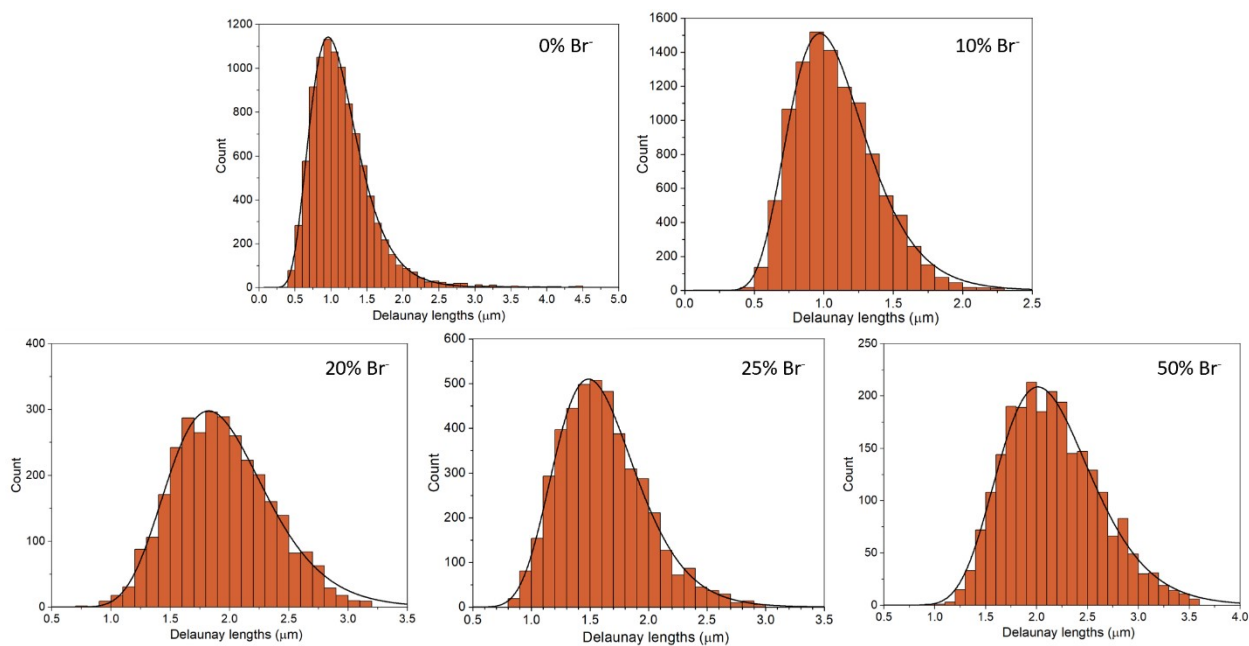

Fig. S8 Histograms of the Delaunay length distributions (center to center distances) of perforations in SiO$_2$ thin films fabricated with 0, 10, 20, 25, and 50 mol% Br$^-$ ion. The solid black lines are fits to a log normal distribution.
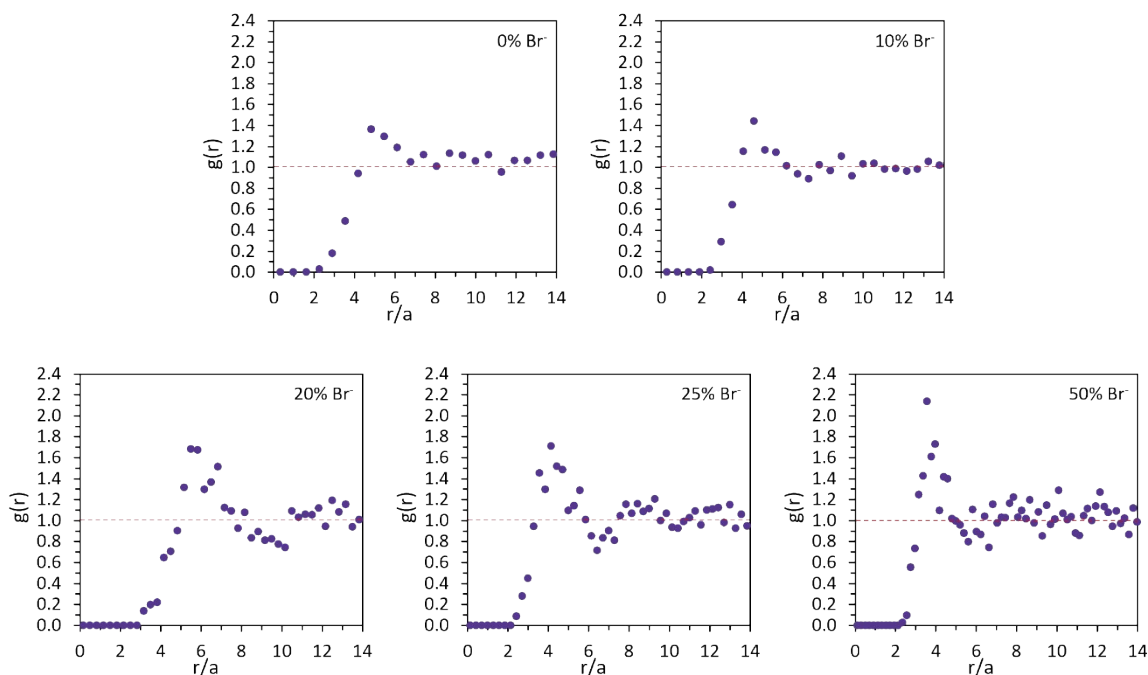
Fig. S9 Pair correlation function $g(r)$, with the mean perforation radius a for samples with 0 (a = 155 nm), 10 (a = 185 nm), 20 (a = 300 nm), 25 (a = 350 nm) and 50 mol% Br$^-$ (a = 490 nm).
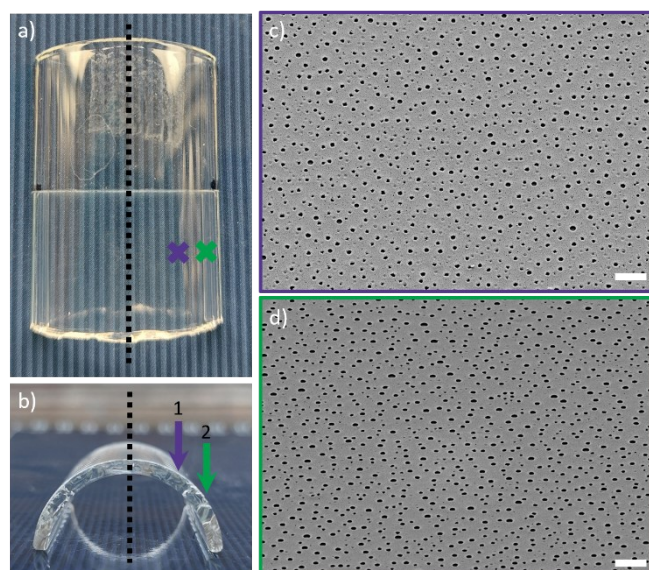

Fig. S10 Observation of a perforated SiO$_2$ layer deposited on a curved borosilicate glass surface by dip-coating, at 1 mm s^{-1} withdrawal speed, under 25°C and 40 % RH with 25 mol% Br$^-$ content. a) Top-view and b) cross-sectional view photographs of the sample under natural light. The dotted black line represents the center of the sample. The two crosses and associated arrows represent the two observation positions for SEM. Position 1 (purple cross and arrow) is located 7 mm from the center. Position 2 (green cross and arrow) is located 11 mm from the center. c-d) SEM images of the perforated SiO$_2$ at c) position 1, with an observation angle of 33° and d) position 2, with an observation angle of 58°. The ellipsoidal shape of the perforations is due to the respective observation angles. Scale bars represent 2 μm, valid for horizontal measurement only. The value of vertical measurement needs to be corrected using the associated observation angle.

Video S1 is provided showing water droplets over the freshly deposited silica layer in real time.

REFERENCES

1 G. L. Drisko, A. Carretero-Genevrier, M. Gich, J. Gàzquez, D. Ferrah, D. Grosso, C. Boissière, J. Rodriguez-Carvajal and C. Sanchez, *Adv. Funct. Mater.*, 2014, **24**, 5494–5502.
2 A. Tsoularis and J. Wallace, *Math. Biosci.*, 2002, **179**, 21–55.